RAA 2019 Vol. **19** No. **4**, 56(12pp) doi: 10.1088/1674–4527/19/4/56

http://www.raa-journal.org *http://iopscience.iop.org/raa*

***R**esearch in*
***A**stronomy and*
***A**strophysics*

New photometric investigation of the low-mass-ratio contact binary star V1853 Orionis

Jia-Jia He[1,2,3], Sheng-Bang Qian[1,2,3,4], Boonrucksar Soonthornthum[5], Amornrat Aungwerojwit[6], Niang-Ping Liu[1,2,3] and Thawicharat Sarotsakulchai[1,2,3,4]

[1] Yunnan Observatories, Chinese Academy of Sciences, Kunming 650216, China; *hjj@ynao.ac.cn*
[2] Key Laboratory of the Structure and Evolution of Celestial Objects, Chinese Academy of Sciences, Kunming 650216, China
[3] Center for Astronomical Mega-Science, Chinese Academy of Sciences, Beijing 100101, China
[4] University of Chinese Academy of Sciences, Beijing 100049, China
[5] National Astronomical Research Institute of Thailand, 191 Siriphanich Bldg. 2nd Fl. Huay Kaew Rd. Suthep District, Muang, Chiang Mai 50200, Thailand
[6] Department of Physics, Faculty of Science, Naresuan University, Phitsanulok 65000, Thailand

Received 2018 August 15; accepted 2018 October 31

Abstract Four-color charge-coupled device (CCD) light curves in the B, V, Rc and Ic bands of the total-eclipsing binary system V1853 Orionis (V1853 Ori) are presented. By comparing our light curves with those published by previous investigators, it is determined that the O'Connell effect on the light curves has disappeared. By analyzing those multi-color light curves with the Wilson-Devinney code (W-D code), it is discovered that V1853 Ori is an A-type intermediate-contact binary with a degree of contact factor of $f = 33.3\%(3.7\%)$ and a mass ratio of $q = 0.1896(0.0013)$. Combining our 10 newly determined times of light minima together with others published in the literature, the period changes of the system are investigated. We found that the general trend of the observed minus calculated $(O-C)$ curve shows a downward parabolic variation that corresponds to a long-term decrease in the orbital period with a rate of $dP/dt = -1.96(0.46) \times 10^{-7}\,\mathrm{d\,yr^{-1}}$. The long-term period decrease could be explained by mass transfer from the more-massive component to the less-massive one. By combining our photometric solutions with data from *Gaia* DR2, absolute parameters were derived as $M_1 = 1.20\,M_\odot$, $M_2 = 0.23\,M_\odot$, $R_1 = 1.36\,R_\odot$ and $R_2 = 0.66\,R_\odot$. The long-term period decrease and intermediate-contact configuration suggest that V1853 Ori will evolve into a high fill-out overcontact binary.

Key words: stars: binaries: close — stars: binaries: eclipsing — stars: individual (V1853 Ori)

1 INTRODUCTION

V1853 Orionis (V1853 Ori = GSC 01283–00053 = NSVS 9553026 = ASAS 051305+155812) was discovered to be a variable star by the Robotic Optical Transient Search Experiment (ROTSE)-I project (Gettel et al. 2006). They demonstrated it was a contact binary candidate by using the observed period-color relation and its binary nature was confirmed by visual examination of the light curves. Later, a total of 236 measurements in the V and R bands were obtained by Blattler & Diethelm (2007). They classified V1853 Ori as an EW-type binary and gave the first linear ephemeris

$$\mathrm{Min.I\ (HJD)} = 2454066.5778 + 0.383004^{\mathrm{d}} \times E \quad (1)$$

based on 12 times of light minima with the ROTSE-I data. Their $V-R$ color curve showed no variation. Samec et al. (2011) published $UBVRcIc$ light curves that were obtained on 2017 December 26, 29, 30 and 31 at Lowell Observatory with the Lowell 31-inch reflector. Their light curves showed positive O'Connell effect (the magnitudes at phase 0.25 are lower than the magnitudes at phase 0.75, O'Connell 1951) in the B, V and Rc bands but negative

Table 1 LAMOST Results for V1853 Ori

Stars	Obs-Date	Sp.	$T_{\rm eff}$ (K)	$\log g$ (cm s^{-2})	[Fe/H] (dex)
V1853 Ori	2014–10–15	F5	6240	4.07	–0.24

Table 2 Coordinates of V1853 Ori, the Comparison Star and the Check Star

Stars	α_{2000}	δ_{2000}
V1853 Ori	$05^{\rm h}13^{\rm m}06.069^{\rm s}$	$+15^\circ58'12.22''$
Comparison star	$05^{\rm h}12^{\rm m}48.08^{\rm s}$	$+15^\circ58'01.8''$
Check star	$05^{\rm h}12^{\rm m}49.98^{\rm s}$	$+15^\circ56'37.4''$

O'Connell effect in the U and Ic bands. The asymmetric light curves were explained by two dark spots on the primary star. Their photometric analysis with the Wilson-Devinney (W-D) code showed that this system is an extreme mass ratio W-type overcontact binary ($q = 0.20$). The derived fill-out factor of $\sim$50% revealed that it is approaching the final stages of its binary star evolution. These properties indicate that V1853 Ori is an interesting target for further investigation. Both components in the binary system may merge into a rapidly rotating single star when it meets the more familiar criterion that the orbital angular momentum is less than 3 times the total spin angular momentum, i.e., $J_{\rm orb} < 3J_{\rm rot}$ (Hut 1980). Therefore, it is a progenitor candidate for luminous red novae (e.g., Zhu et al. 2016).

Samec et al. (2011) revised the linear ephemeris as

$$\mathrm{Min.I\ (HJD)} = 2454066.57858 + 0.38300155^{\rm d} \times E. \quad (2)$$

They showed that the period of V1853 Ori is not variable. Recently, V1853 Ori was observed by the Large Sky Area Multi-Object Fiber Spectroscopic Telescope (LAMOST) survey on 2014 October 15. Stellar atmospheric parameters of the binary were published by Qian et al. (2017a) and are listed in Table 1. Distributions of the metallicity ([Fe/H]) and the gravitational acceleration $\log g$ for EW-types were given by Qian et al. (2018). It was demonstrated that the values of V1853 Ori are close to the peaks of the distributions. Moreover, the period (0.38 d) of this system is also close to the peak of the period distribution given by Qian et al. (2017a). These reveal that V1853 Ori is a typical EW-type binary. This eclipsing binary was also included in *Gaia* Data Release 2 (Gaia Collaboration et al. 2018) and the parallax (π = 2.6856(0.0465)mas) was given.

2 MULTI-COLOR CCD PHOTOMETRIC OBSERVATIONS

New photometric observations of V1853 Ori were carried out in the B, V, Rc and Ic bands with the DW436 2048 × 2048 charge-coupled device (CCD) photometric system attached to the 1-m reflecting telescope operated by Yunnan Observatories in China over three nights on 2012 February 6, 7 and 8 . The effective field of view of the photometric system was $7' \times 7'$ at the Cassegrain focus. The integration times were 120 s for the B band, 60 s for the V band, 30 s for the Rc band and 20 s for the Ic band during our observation. The comparison star and check star are in the same field of view on the CCD camera. One of images of the B band is shown in Figure 1.

The coordinates of V1853 Ori, and those of the comparison and check stars are listed in Table 2. PHOT (measuring magnitudes for a list of stars), from the IRAF aperture photometry package, was used to reduce the observed images. Photometric data in the B, V, Rc and Ic bands together with their Heliocentric Julian Dates (HJDs) are listed in Tables 3, 4, 5 and 6, respectively. The complete CCD light curves in the B, V, Rc and Ic bands with respect to the linear ephemeris,

$$\mathrm{Min.I\ (HJD)} = 2455965.11174 + 0.38300155^{\rm d} \times E, \quad (3)$$

are shown in Figure 2. The magnitude differences between the comparison and check stars are also displayed in the lower panel of this figure. The epoch in Equation (3) is obtained by us and the period is from Samec et al. (2011).

Apart from the 1-m reflecting telescope operated by Yunnan Observatories, we also used the 0.4-m telescope at Naresuan University in Thailand and the 60-cm Ritchey-Chrétien (R-C) reflecting telescope operated by Yunnan Observatories in China. By applying the least-squares parabolic fitting method, 30 CCD times of light minima, averaged into 10 mean eclipse times, are listed in Table 7.

3 ORBITAL PERIOD INVESTIGATION

Since the variable was discovered by Gettel et al. (2006), the period changes have been investigated only by Samec et al. (2011), and their study shows no variation. Diethelm (2011) and Diethelm (2012) published two times of light minima for V1853 Ori. To study the variations in orbital period, we collect all the available photoelectric and CCD times of light minima from websites and the literature. All the primary and secondary times of light minima are listed in Table 8. The $(O-C)$ values (observational times of light minima minus calculated times of light minima) calculated by Equation (3) are listed in the third column of Table 8 and plotted in the upper panel of Figure 3. In this figure, black solid dots refer to data from Samec et al. (2011), red solid dots indicate data obtained by Diethelm (2011)

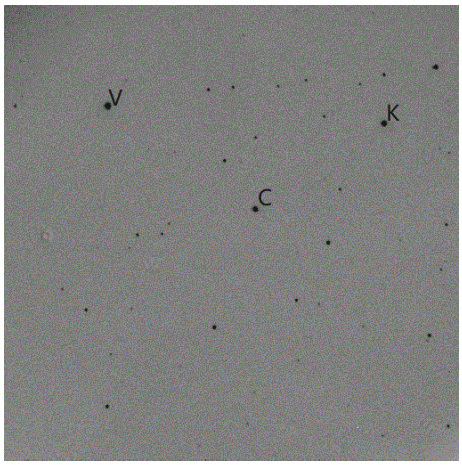

Fig. 1 One CCD image of V1853 Ori obtained by the 1-m reflecting telescope at Yunnan Observatories, including variable (V), comparison (C) and check (K) stars.

Table 3 CCD Photometric Data for V1853 Ori in the B Band

JD (Hel.) 2459000+	$\Delta(m)$	JD (Hel.) 2455900+	$\Delta(m)$	JD (Hel.) 2455900+	$\Delta(m)$	JD (Hel.) 2455900+	$\Delta(m)$	JD (Hel.) 2455900+	$\Delta(m)$	JD (Hel.) 2455900+	$\Delta(m)$
63.98427	−0.901	64.07744	−1.200	64.17892	−0.905	65.07344	−1.048	65.19654	−1.220	66.09014	−0.889
63.98746	−0.914	64.07981	−1.197	64.18211	−0.949	65.07662	−1.024	65.19973	−1.228	66.09333	−0.932
63.98982	−0.951	64.08217	−1.183	64.18529	−0.972	65.07981	−1.004	65.20292	−1.223	66.09652	−0.943
63.99219	−0.973	64.08536	−1.186	64.18848	−0.987	65.08299	−0.954	65.97859	−1.244	66.09970	−0.987
63.99455	−1.011	64.08773	−1.186	64.19167	−1.025	65.08618	−0.942	65.98178	−1.225	66.10289	−1.008
63.99692	−1.014	64.09009	−1.162	64.19485	−1.043	65.08937	−0.905	65.98496	−1.209	66.10608	−1.042
63.99928	−1.041	64.09246	−1.168	64.19804	−1.091	65.09255	−0.869	65.98818	−1.216	66.10926	−1.032
64.00165	−1.048	64.09482	−1.157	64.20122	−1.094	65.09574	−0.843	65.99137	−1.189	66.11245	−1.081
64.00402	−1.062	64.09719	−1.143	64.20441	−1.092	65.09893	−0.838	65.99456	−1.181	66.11563	−1.093
64.00638	−1.086	64.09955	−1.137	64.98103	−1.162	65.10211	−0.817	65.99774	−1.180	66.11882	−1.118
64.00875	−1.110	64.10192	−1.124	64.98422	−1.177	65.10530	−0.839	66.00093	−1.169	66.12201	−1.122
64.01193	−1.129	64.10429	−1.118	64.98741	−1.170	65.10849	−0.810	66.00411	−1.166	66.12519	−1.148
64.01430	−1.138	64.10665	−1.102	64.99059	−1.197	65.11167	−0.810	66.00730	−1.152	66.12838	−1.155
64.01666	−1.150	64.10984	−1.085	64.99378	−1.216	65.11486	−0.812	66.01049	−1.139	66.13157	−1.175
64.01903	−1.152	64.11220	−1.053	64.99697	−1.208	65.11804	−0.843	66.01367	−1.123	66.13475	−1.152
64.02139	−1.161	64.11457	−1.057	65.00015	−1.220	65.12123	−0.833	66.01686	−1.117	66.13794	−1.183
64.02376	−1.176	64.11693	−1.029	65.00334	−1.220	65.12463	−0.837	66.02004	−1.109	66.14113	−1.193
64.02612	−1.187	64.11930	−1.026	65.00652	−1.232	65.12781	−0.839	66.02323	−1.094	66.14431	−1.205
64.02849	−1.202	64.12167	−1.003	65.00971	−1.227	65.13100	−0.890	66.02642	−1.085	66.14750	−1.213
64.03086	−1.191	64.12403	−0.979	65.01290	−1.235	65.13419	−0.891	66.02960	−1.053	66.15083	−1.214
64.03322	−1.199	64.12640	−0.959	65.01608	−1.238	65.13737	−0.932	66.03279	−1.023	66.15402	−1.232
64.03641	−1.202	64.12877	−0.931	65.01927	−1.242	65.14056	−0.952	66.03598	−0.995	66.15721	−1.219
64.03877	−1.207	64.13114	−0.917	65.02245	−1.240	65.14375	−1.002	66.03916	−0.971	66.16039	−1.236
64.04114	−1.224	64.13432	−0.877	65.02564	−1.236	65.14693	−1.010	66.04235	−0.945	66.16421	−1.227
64.04350	−1.222	64.13669	−0.868	65.02883	−1.231	65.15012	−1.053	66.04554	−0.930	66.16740	−1.223
64.04587	−1.230	64.13905	−0.857	65.03201	−1.232	65.15331	−1.073	66.04872	−0.891	66.17058	−1.226
64.04824	−1.228	64.14142	−0.854	65.03520	−1.221	65.15649	−1.097	66.05191	−0.868	66.17377	−1.226
64.05060	−1.219	64.14378	−0.831	65.03839	−1.221	65.15968	−1.127	66.05509	−0.843	66.17696	−1.212
64.05297	−1.228	64.14615	−0.840	65.04157	−1.222	65.16286	−1.136	66.05828	−0.869	66.18014	−1.209
64.05533	−1.252	64.14852	−0.852	65.04476	−1.190	65.16718	−1.149	66.06147	−0.855	66.18333	−1.198
64.05770	−1.240	64.15088	−0.834	65.04794	−1.187	65.17037	−1.152	66.06465	−0.859	66.18652	−1.218
64.06088	−1.247	64.15607	−0.839	65.05113	−1.170	65.17356	−1.179	66.06784	−0.841	66.18970	−1.212
64.06325	−1.230	64.15967	−0.856	65.05432	−1.163	65.17674	−1.173	66.07103	−0.849	66.19289	−1.189
64.06561	−1.232	64.16285	−0.838	65.05750	−1.145	65.17993	−1.193	66.07421	−0.843	66.19607	−1.166
64.06798	−1.216	64.16604	−0.845	65.06069	−1.122	65.18312	−1.197	66.07740	−0.851	66.19926	−1.127
64.07035	−1.229	64.16922	−0.863	65.06388	−1.108	65.18630	−1.211	66.08058	−0.849	66.20245	−1.160
64.07271	−1.215	64.17241	−0.879	65.06706	−1.104	65.19017	−1.202	66.08377	−0.856		
64.07508	−1.210	64.17560	−0.885	65.07025	−1.061	65.19336	−1.223	66.08696	−0.853		

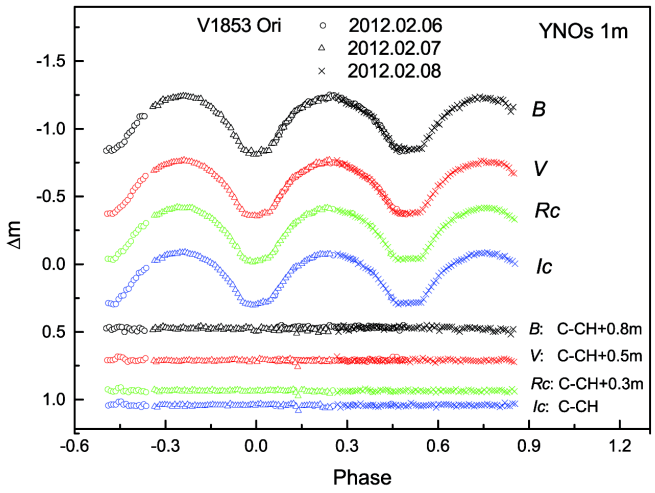

Fig. 2 CCD photometric light curves in the B and V bands obtained using the 1-m telescope at Yunnan Observatories in 2012. The magnitude differences between the comparison and check stars are shown in the lower panel.

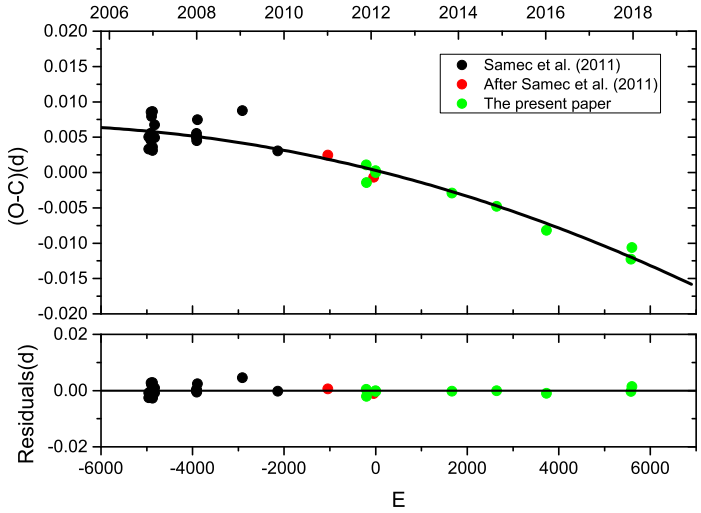

Fig. 3 $(O-C)$ diagram of the short-period close binary V1853 Ori based on all the available primary and secondary photoelectric and CCD times of light minima. The quadratic fit (*black solid line*) shows a long-term period decrease. Residuals with respect to the quadratic ephemerides are displayed in the *lower panel*. *Black solid dots* refer to data from Samec et al. (2011), *red solid dots* indicate data obtained by Diethelm (2011) and Diethelm (2012), and *green solid dots* signify data obtained by us.

and Diethelm (2012), and green solid dots signify data obtained by us. A least-squares solution yields the following ephemeris

$$\begin{aligned}(O-C) =& 2455965.11204(0.00046) \\ &+ 0.38299992^{\mathrm{d}}(0.00000008^{\mathrm{d}}) \times E \\ &- 1.03(0.24) \times 10^{-10} E^2.\end{aligned} \quad (4)$$

With the quadratic term of this ephemeris, a continuous period decrease, at a rate of $dP/dt = -1.96(0.46) \times 10^{-7}\,\mathrm{d\,yr^{-1}}$, is determined. The residuals from Equation (4) are shown in the lower panel of Figure 3 and listed in column 4 of Table 8.

4 PHOTOMETRIC SOLUTIONS

To understand its geometrical structure and evolutionary state, the B, V, Rc and Ic light curves shown in Figure 2 were analyzed using the W-D code (Wilson & Devinney 1971; Wilson & Van Hamme 2003; Wilson et al. 2010; van Hamme 1993). The light curves published by Samec et al. (2011) were asymmetric and showed the O'Connell effect that could be explained by dark spot activity on the cool component (e.g., Qian et al. 2017b). However, the light curves displayed in Figure 2 are almost symmetric and show typical EW-type variations, which enable deter-

Table 4 CCD Photometric Data for V1853 Ori in the V Band

JD (Hel.) 2455900+	$\Delta(m)$	JD (Hel.) 2455900+	$\Delta(m)$	JD (Hel.) 2455900+	$\Delta(m)$	JD (Hel.) 2455900+	$\Delta(m)$	JD (Hel.) 2455900+	$\Delta(m)$	JD (Hel.) 2455900+	$\Delta(m)$
63.98544	−0.429	64.07861	−0.717	64.18009	−0.457	65.07460	−0.569	65.19771	−0.753	66.09131	−0.439
63.98862	−0.466	64.08098	−0.712	64.18327	−0.475	65.07779	−0.545	65.20090	−0.765	66.09450	−0.452
63.99099	−0.494	64.08334	−0.714	64.18646	−0.504	65.08097	−0.515	65.20408	−0.769	66.09768	−0.491
63.99336	−0.504	64.08653	−0.700	64.18965	−0.543	65.08416	−0.491	65.97975	−0.768	66.10087	−0.519
63.99572	−0.537	64.08889	−0.688	64.19283	−0.567	65.08735	−0.451	65.98294	−0.746	66.10406	−0.538
63.99809	−0.545	64.09126	−0.684	64.19602	−0.585	65.09053	−0.420	65.98613	−0.735	66.10724	−0.579
64.00045	−0.559	64.09363	−0.676	64.19921	−0.615	65.09372	−0.402	65.98935	−0.741	66.11043	−0.589
64.00282	−0.597	64.09599	−0.666	64.20239	−0.629	65.09691	−0.370	65.99254	−0.729	66.11362	−0.608
64.00519	−0.605	64.09836	−0.654	64.20558	−0.652	65.10009	−0.365	65.99572	−0.712	66.11680	−0.624
64.00755	−0.626	64.10072	−0.651	64.98220	−0.690	65.10328	−0.357	65.99891	−0.705	66.11999	−0.650
64.00992	−0.635	64.10309	−0.631	64.98539	−0.697	65.10647	−0.358	66.00209	−0.698	66.12318	−0.665
64.01310	−0.645	64.10545	−0.633	64.98857	−0.714	65.10965	−0.359	66.00528	−0.683	66.12636	−0.677
64.01547	−0.662	64.10782	−0.617	64.99176	−0.724	65.11284	−0.354	66.00847	−0.676	66.12955	−0.690
64.01783	−0.667	64.11100	−0.597	64.99495	−0.733	65.11602	−0.361	66.01165	−0.655	66.13273	−0.701
64.02020	−0.682	64.11337	−0.583	64.99813	−0.737	65.11921	−0.375	66.01484	−0.647	66.13592	−0.700
64.02256	−0.684	64.11574	−0.571	65.00132	−0.742	65.12240	−0.381	66.01803	−0.641	66.13911	−0.716
64.02493	−0.697	64.11810	−0.557	65.00450	−0.751	65.12580	−0.376	66.02121	−0.626	66.14229	−0.724
64.02729	−0.700	64.12047	−0.531	65.00769	−0.755	65.12898	−0.388	66.02440	−0.608	66.14548	−0.726
64.02966	−0.712	64.12284	−0.516	65.01088	−0.756	65.13217	−0.419	66.02758	−0.580	66.14867	−0.737
64.03202	−0.722	64.12520	−0.487	65.01406	−0.756	65.13535	−0.446	66.03077	−0.564	66.15200	−0.739
64.03439	−0.729	64.12757	−0.473	65.01725	−0.764	65.13854	−0.477	66.03396	−0.535	66.15519	−0.743
64.03757	−0.732	64.12994	−0.457	65.02044	−0.769	65.14173	−0.506	66.03714	−0.518	66.15838	−0.740
64.03994	−0.740	64.13230	−0.433	65.02362	−0.760	65.14491	−0.532	66.04033	−0.495	66.16156	−0.763
64.04231	−0.742	64.13549	−0.419	65.02681	−0.758	65.14810	−0.561	66.04352	−0.462	66.16538	−0.762
64.04467	−0.744	64.13786	−0.392	65.03000	−0.757	65.15129	−0.586	66.04670	−0.430	66.16856	−0.748
64.04704	−0.744	64.14022	−0.408	65.03318	−0.746	65.15447	−0.605	66.04989	−0.404	66.17175	−0.748
64.04940	−0.755	64.14259	−0.375	65.03637	−0.744	65.15766	−0.641	66.05308	−0.389	66.17494	−0.753
64.05177	−0.751	64.14495	−0.379	65.03955	−0.736	65.16084	−0.650	66.05626	−0.384	66.17812	−0.755
64.05414	−0.752	64.14732	−0.370	65.04274	−0.724	65.16403	−0.658	66.05945	−0.378	66.18131	−0.749
64.05650	−0.745	64.14968	−0.376	65.04593	−0.721	65.16835	−0.677	66.06263	−0.376	66.18449	−0.741
64.05887	−0.752	64.15205	−0.368	65.04911	−0.705	65.17154	−0.687	66.06582	−0.378	66.18768	−0.747
64.06205	−0.750	64.15724	−0.372	65.05230	−0.691	65.17472	−0.694	66.06901	−0.375	66.19087	−0.738
64.06442	−0.748	64.16083	−0.376	65.05549	−0.683	65.17791	−0.713	66.07219	−0.370	66.19406	−0.725
64.06678	−0.748	64.16402	−0.373	65.05867	−0.660	65.18110	−0.715	66.07538	−0.383	66.19724	−0.712
64.06915	−0.741	64.16720	−0.383	65.06186	−0.645	65.18428	−0.730	66.07856	−0.378	66.20043	−0.675
64.07151	−0.741	64.17039	−0.403	65.06504	−0.627	65.18747	−0.750	66.08175	−0.382	66.20361	−0.671
64.07388	−0.734	64.17358	−0.420	65.06823	−0.616	65.19134	−0.751	66.08494	−0.385		
64.07624	−0.730	64.17676	−0.435	65.07142	−0.590	65.19452	−0.742	66.08812	−0.404		

mining reliable photometric parameters. Magnitudes in the J, H and K bands (10.46, 10.20 and 10.10 mag respectively) were obtained from 2MASS (Cutri et al. 2003). The color indexes $J - H = 0.26$ mag and $H - K = 0.10$ mag indicate that the spectral type of V1853 Ori is F6 or K3. The corresponding effective temperatures are estimated as 6400 K or 4800 K (Drilling & Landolt 2000), which are quite different. The effective temperature (6240 K) obtained by LAMOST is in that range. Therefore, during the solution process, the effective temperature of star 1 was chosen as $T_1 = 6240$ K. As shown in Figure 2, the depths of both minima are nearly the same, indicating nearly the same temperature for both components. Therefore, we take the same values of the gravity-darkening coefficients and the bolometric albedo for both components, i.e., g_1 = g_2 = 0.32 (Lucy 1967) and A_1 = A_2 = 0.5 (Ruciński 1969). The limb-darkening coefficients were used according to Claret & Gimenez (1990) (x and y are the bolometric and bandpass limb-darkening coefficients respectively). The adjustable parameters include: orbital inclination (i); mean temperature of star 2 (T_2); monochromatic luminosity of star 1 (L_{1B}, L_{1V}, L_{1Rc}, L_{1Ic}); and dimensionless potential of star 1 ($\Omega_1 = \Omega_2$, mode 3 for overcontact configuration).

Table 5 CCD Photometric Data for V1853 Ori in the Rc Band

JD (Hel.) 2455900+	$\Delta(m)$	JD (Hel.) 2455900+	$\Delta(m)$	JD (Hel.) 2455900+	$\Delta(m)$	JD (Hel.) 2455900+	$\Delta(m)$	JD (Hel.) 2455900+	$\Delta(m)$	JD (Hel.) 2455900+	$\Delta(m)$
63.98608	−0.095	64.99878	−0.402	65.08800	−0.126	65.17856	−0.369	66.04098	−0.147	66.13020	−0.363
64.01056	−0.294	65.00197	−0.401	65.09118	−0.077	65.18175	−0.378	66.04416	−0.125	66.13338	−0.356
64.03503	−0.380	65.00515	−0.407	65.09437	−0.051	65.18493	−0.388	66.04735	−0.084	66.13657	−0.358
64.05951	−0.407	65.00834	−0.412	65.09755	−0.038	65.18867	−0.404	66.05054	−0.061	66.13975	−0.369
64.08399	−0.376	65.01153	−0.421	65.10074	−0.022	65.19199	−0.408	66.05372	−0.043	66.14294	−0.381
64.10846	−0.281	65.01471	−0.419	65.10393	−0.028	65.19517	−0.400	66.05691	−0.033	66.14613	−0.391
64.13295	−0.076	65.01790	−0.413	65.10711	−0.015	65.19836	−0.415	66.06010	−0.042	66.14931	−0.397
64.15788	−0.040	65.02108	−0.413	65.11030	−0.019	65.20154	−0.416	66.06328	−0.034	66.15265	−0.399
64.16148	−0.039	65.02427	−0.414	65.11349	−0.026	65.20473	−0.409	66.06647	−0.040	66.15584	−0.406
64.16467	−0.033	65.02746	−0.416	65.11667	−0.024	65.98041	−0.401	66.06965	−0.043	66.15902	−0.415
64.16785	−0.045	65.03064	−0.417	65.11986	−0.037	65.98359	−0.395	66.07284	−0.041	66.16221	−0.411
64.17104	−0.074	65.03383	−0.406	65.12305	−0.044	65.98682	−0.387	66.07603	−0.039	66.16603	−0.416
64.17423	−0.094	65.03701	−0.395	65.12644	−0.043	65.99000	−0.380	66.07921	−0.045	66.16921	−0.416
64.17741	−0.096	65.04020	−0.387	65.12963	−0.060	65.99319	−0.380	66.08240	−0.040	66.17240	−0.415
64.18073	−0.124	65.04339	−0.374	65.13282	−0.084	65.99637	−0.376	66.08558	−0.043	66.17558	−0.411
64.18392	−0.148	65.04657	−0.368	65.13600	−0.110	65.99956	−0.365	66.08877	−0.060	66.17877	−0.413
64.18711	−0.169	65.04976	−0.350	65.13919	−0.147	66.00274	−0.352	66.09196	−0.096	66.18196	−0.400
64.19029	−0.218	65.05295	−0.349	65.14238	−0.171	66.00593	−0.345	66.09515	−0.125	66.18514	−0.404
64.19348	−0.231	65.05613	−0.336	65.14556	−0.201	66.00911	−0.344	66.09833	−0.149	66.18833	−0.388
64.19667	−0.255	65.05932	−0.320	65.14875	−0.221	66.01230	−0.322	66.10152	−0.187	66.19152	−0.389
64.19985	−0.281	65.06251	−0.297	65.15193	−0.249	66.01549	−0.317	66.10470	−0.208	66.19470	−0.362
64.20304	−0.279	65.06569	−0.284	65.15512	−0.272	66.01867	−0.297	66.10789	−0.233	66.19789	−0.357
64.20623	−0.303	65.06888	−0.258	65.15831	−0.297	66.02186	−0.284	66.11108	−0.255	66.20108	−0.340
64.98285	−0.360	65.07206	−0.247	65.16149	−0.311	66.02505	−0.265	66.11426	−0.279	66.20426	−0.330
64.98604	−0.362	65.07525	−0.223	65.16468	−0.318	66.02823	−0.242	66.11745	−0.289		
64.98922	−0.369	65.07844	−0.201	65.16900	−0.339	66.03142	−0.219	66.12064	−0.305		
64.99241	−0.384	65.08162	−0.167	65.17219	−0.356	66.03460	−0.208	66.12382	−0.325		
64.99559	−0.387	65.08481	−0.139	65.17537	−0.370	66.03779	−0.174	66.12701	−0.328		

A q-search ($q = M_2/M_1$) method was used to determine the mass ratio of the system. Solutions were carried out for a series of values of the mass ratio. For each value of q, the calculation started at mode 2 (detached mode) and we found that the solutions usually converged to mode 3. The relation between the resulting sum $\Sigma W_i(O-C)_i^2$ of weighted square deviations and q is plotted in Figure 4. As shown in the figure, two minima are found at $q = 0.18$ and $q = 5.6$ respectively. They are the inverses of each other. The $\Sigma W_i(O-C)_i^2$ value at $q = 0.18$ is less than that at $q = 5.6$. Therefore, we chose the initial value of q as 0.18 and made it an adjustable parameter. Then we performed a differential correction until it converged and final solutions were derived. The solution converged at $q = 0.1896(0.0013)$. The photometric solutions are listed in column 2 of Table 9 and the theoretical light curves computed with those photometric parameters are plotted in Figure 5. The light curves are nearly symmetric and no spotted solution is needed. The solution reveals that V1853 Ori is an A-type intermediate contact binary with a degree of contact factor of $f = 33.3\%(3.7\%)$ and a mass ratio of $q = 0.1896(0.0013)$. The geometrical structures at phases 0.0, 0.25, 0.5 and 0.75 are shown in Figure 6.

5 DISCUSSION AND CONCLUSIONS

The light curves of V1853 Ori published by Samec et al. (2011) are asymmetric and manifest the O'Connell effect. However, when we observed it in 2012, the light curves were symmetric and the O'Connell effect had disappeared. A comparison of the two sets of light curves is displayed in Figure 7. It is evident that the maxima at phase 0.25 in the light curves of Samec et al. (2011) are slightly higher than those at phase 0.75, while the two maxima in our light curves are nearly equal. Moreover, as exhibited in the figure, the light curves obtained by Samec et al. (2011) display a larger scatter. These indicate that our light curves could be used to determine more reliable solutions.

Samec et al. (2011) used two dark spots on the primary component to explain the asymmetries of their light curves. Their results indicated that V1853 Ori is an extreme mass

Table 6 CCD Photometric Data for V1853 Ori in the Ic Band

JD (Hel.) 2455900+	$\Delta(m)$	JD (Hel.) 2455900+	$\Delta(m)$	JD (Hel.) 2455900+	$\Delta(m)$	JD (Hel.) 2455900+	$\Delta(m)$	JD (Hel.) 2455900+	$\Delta(m)$	JD (Hel.) 2455900+	$\Delta(m)$
63.98650	0.233	64.99920	−0.071	65.08841	0.217	65.17898	−0.040	66.04139	0.182	66.13061	−0.020
64.01098	0.032	65.00238	−0.072	65.09160	0.250	65.18216	−0.045	66.04458	0.209	66.13380	−0.021
64.03545	−0.051	65.00557	−0.074	65.09479	0.278	65.18535	−0.062	66.04777	0.241	66.13698	−0.033
64.05993	−0.066	65.00875	−0.079	65.09797	0.291	65.18909	−0.066	66.05095	0.265	66.14017	−0.037
64.08440	−0.038	65.01194	−0.077	65.10116	0.296	65.19240	−0.075	66.05414	0.286	66.14336	−0.049
64.10888	0.061	65.01513	−0.087	65.10434	0.298	65.19559	−0.073	66.05733	0.296	66.14654	−0.063
64.13337	0.246	65.01831	−0.086	65.10753	0.304	65.19877	−0.070	66.06051	0.288	66.14973	−0.074
64.15830	0.288	65.02150	−0.089	65.11072	0.301	65.20196	−0.075	66.06370	0.288	66.15307	−0.067
64.16190	0.290	65.02469	−0.082	65.11390	0.292	65.20515	−0.074	66.06688	0.284	66.15625	−0.077
64.16508	0.296	65.02787	−0.075	65.11709	0.289	65.98082	−0.076	66.07007	0.292	66.15944	−0.082
64.16827	0.295	65.03106	−0.071	65.12028	0.277	65.98401	−0.066	66.07326	0.284	66.16263	−0.080
64.17146	0.258	65.03424	−0.070	65.12346	0.283	65.98723	−0.063	66.07644	0.285	66.16644	−0.082
64.17464	0.234	65.03743	−0.061	65.12686	0.276	65.99042	−0.056	66.07963	0.283	66.16963	−0.087
64.17783	0.231	65.04062	−0.054	65.13005	0.262	65.99360	−0.048	66.08281	0.282	66.17281	−0.076
64.18115	0.189	65.04380	−0.038	65.13323	0.232	65.99679	−0.042	66.08600	0.284	66.17600	−0.073
64.18434	0.182	65.04699	−0.032	65.13642	0.207	65.99997	−0.032	66.08919	0.260	66.17919	−0.072
64.18752	0.149	65.05018	−0.025	65.13961	0.179	66.00316	−0.027	66.09237	0.222	66.18237	−0.078
64.19071	0.117	65.05336	−0.014	65.14279	0.158	66.00634	−0.001	66.09556	0.193	66.18556	−0.059
64.19390	0.100	65.05655	−0.001	65.14598	0.130	66.00953	−0.011	66.09875	0.169	66.18875	−0.055
64.19708	0.065	65.05974	0.008	65.14916	0.102	66.01272	0.016	66.10194	0.137	66.19193	−0.060
64.20027	0.059	65.06292	0.029	65.15235	0.083	66.01590	0.028	66.10512	0.123	66.19512	−0.037
64.20346	0.042	65.06611	0.046	65.15554	0.053	66.01909	0.037	66.10831	0.087	66.19831	−0.029
64.20664	0.028	65.06929	0.070	65.15872	0.027	66.02228	0.048	66.11150	0.065	66.20149	−0.022
64.98327	−0.026	65.07248	0.090	65.16191	0.016	66.02546	0.063	66.11468	0.047	66.20468	−0.003
64.98645	−0.027	65.07567	0.109	65.16509	0.015	66.02865	0.083	66.11787	0.035		
64.98964	−0.045	65.07885	0.133	65.16942	−0.001	66.03184	0.110	66.12105	0.021		
64.99282	−0.042	65.08204	0.154	65.17260	−0.020	66.03502	0.136	66.12424	0.010		
64.99601	−0.062	65.08522	0.191	65.17579	−0.030	66.03821	0.157	66.12743	−0.006		

ratio ($q = 0.2$) W-type contact binary with a fill-out factor of ∼50%. By analyzing our light curves obtained by the 1.0-m reflecting telescope at Yunnan Observatories with the W-D code, we found that V1853 Ori is an A-type contact binary with a mass ratio $q = 0.1896$ that is slightly smaller than the value $q = 0.20$ obtained by Samec et al. (2011). However, the fill-out factor we derived is 33.3%, which is much smaller than 50% obtained by Samec et al. (2011). The photometric results of Samec et al. (2011) demonstrated that the temperature of the less-massive component is about 61 K higher than the more-massive one, while our photometric results indicate that the temperature of the less-massive component is only 3 K lower than the more-massive one. We think that our results are more credible because they are based on high-precision B, V, Rc and Ic bands and symmetric CCD light curves. It is possible that the two cool magnetic spots on the primary component had disappeared when we observed it. Perhaps the asymmetric light curves affected the photometry results. The conclusion, identification of W-type, obtained by Samec et al. (2011) may be caused by the two cool spots modeled on the primary component. We think that exchange between A-type and W-type can be explained by activity of some dark spots on the primary component, as pointed out by Binnendijk (1964). Such phenomena have also been encountered in other W UMa binaries such as RZ Com (He & Qian 2008) and FG Hya (Qian & Yang 2005).

The absolute magnitude of V1853 Ori in the V band is estimated as 3.67 mag by using the relation $M_V = m_V - 5\log(1000/\pi) + 5 - A_V$ (e.g., Chen et al. 2018), where the values of m_V, the parallax π and A_V are chosen as 11.60(0.16) mag (Høg et al. 2000), 2.6856(0.0465) mas (Gaia Collaboration et al. 2018) and 0.075(0.025) mag (Chen et al. 2018), respectively. The period and luminosity of V1853 Ori are in good agreement with the period-luminosity relation given by Chen et al. (2018). The total luminosity of the two components should be 2.964 $L_\odot$ based on the equation $M_{\rm bol} = -2.5\log L/L_\odot + 4.74$ and the bolometric correction BC $= M_{\rm bol} - M_V = -0.11$ (Drilling & Landolt 2000), where $L_\odot = 3.845 \times$

Table 7 New CCD Times of Light Minima for V1853 Ori

No.	JD (Hel.)	Error (d)	Method	Min.	Filter	Tel.
1	2455886.78873	0.00049	CCD	II	B	Thai-0.4m
	2455886.78886	0.00026	CCD	II	V	Thai-0.4m
	2455886.78917	0.00049	CCD	II	Rc	Thai-0.4m
	2455886.78932	0.00037	CCD	II	Ic	Thai-0.4m
Mean	2455886.78902		CCD	II		Thai-0.4m
2	2455887.74322	0.00028	CCD	I	B	Thai-0.4m
	2455887.74400	0.00033	CCD	I	V	Thai-0.4m
	2455887.74434	0.00018	CCD	I	Rc	Thai-0.4m
	2455887.74448	0.00026	CCD	I	Ic	Thai-0.4m
Mean	2455887.74401		CCD	I		Thai-0.4m
3	2455964.15425	0.00026	CCD	II	B	YNOs-1m
	2455964.15473	0.00027	CCD	II	V	YNOs-1m
Mean	2455964.15449		CCD	II		YNOs-1m
4	2455965.11158	0.00029	CCD	I	B	YNOs-1m
	2455965.11163	0.00023	CCD	I	V	YNOs-1m
	2455965.11191	0.00022	CCD	I	Rc	YNOs-1m
	2455965.11185	0.00028	CCD	I	Ic	YNOs-1m
Mean	2455965.11174		CCD	I		YNOs-1m
5	2455966.06929	0.00035	CCD	II	B	YNOs-1m
	2455966.06934	0.00039	CCD	II	V	YNOs-1m
	2455966.06917	0.00032	CCD	II	Rc	YNOs-1m
	2455966.06916	0.00031	CCD	II	Ic	YNOs-1m
Mean	2455966.06924		CCD	II		YNOs-1m
6	2456603.19052	0.00027	CCD	I	I	YNOs-1m
	2456603.18858	0.00031	CCD	I	N	YNOs-1m
	2456603.18920	0.00020	CCD	I	Rc	YNOs-1m
Mean	2456603.18943		CCD			YNOs-60cm
7	2456976.23016	0.00035	CCD	I	Ic	YNOs-60cm
	2456976.23196	0.00041	CCD	I	Rc	YNOs-60cm
Mean	2456976.23106		CCD			YNOs-60cm
8	2457394.08111	0.00140	CCD	I	Ic	YNOs-60cm
	2457394.08361	0.00043	CCD	I	Rc	YNOs-60cm
Mean	2457394.08236		CCD			YNOs-60cm
9	2458100.14243	0.00027	CCD	II	Rc	YNOs-60cm
	2458100.14083	0.00029	CCD	II	V	YNOs-60cm
Mean	2458100.14163		CCD			YNOs-60cm
10	2458109.14383	0.00015	CCD	I	V	YNOs-1m
	2458109.14383	0.00019	CCD	I	Rc	YNOs-1m
	2458109.14379	0.00016	CCD	I	Ic	YNOs-1m
Mean	2458109.14382		CCD			YNOs-1m

Notes: Tel.: Thai-0.4-m: 0.4 m telescope, Naresuan University, Thailand. YNOs-1m: 1.0 m R-C reflecting telescope, Yunnan Observatories, Chinese Academy of Sciences, China. YNOs-60cm: 60 cm R-C reflecting telescope, Yunnan Observatories, Chinese Academy of Sciences, China.

10^{33} erg s^{-1} and +4.74 is the absolute bolometric magnitude of the Sun. The luminosity of the primary component is calculated to be $2.964 \times 0.81214 = 2.407\,L_{\odot}$, while that of the second component is $0.557\,L_{\odot}$. The mass of the primary component should be $1.20\,M_{\odot}$ based on the equation $\log L/L_{\odot} = 3.8 \log M/M_{\odot} + 0.08$ (Drilling & Landolt 2000). Then the mass of the second component is calculated as $M_2 = 0.23\,M_{\odot}$ based on our mass ratio. By using Kepler's third law, the semi-major axis of the binary is derived as $2.50\,R_{\odot}$. Finally, the radii of components R_1 and R_2 are computed as $1.36\,R_{\odot}$ and $0.66\,R_{\odot}$, respectively.

By monitoring V1853 Ori for about six years, 10 times of light minima were obtained. A period analysis with all available eclipse times shows that the period of V1853 Ori

Table 8 $(O-C)$ Values of Light Minima Times for V1853 Ori

JD (Hel.)	Cycles	$(O-C)$	Residual	Reference
2454848.6710	−2915	0.00878	0.00461	Diethelm (2009)
2455144.9170	−2141.5	0.00308	−0.00022	Diethelm (2010)
2454066.3849	−4957.5	0.00334	−0.00249	Diethelm (2007)
2454066.5781	−4957	0.00504	−0.00079	Diethelm (2007)
2454083.4307	−4913	0.00558	−0.00023	Blattler & Diethelm (2007)
2454083.6212	−4912.5	0.00457	−0.00123	Blattler & Diethelm (2007)
2454085.3487	−4908	0.00857	0.00276	Blattler & Diethelm (2007)
2454085.5363	−4907.5	0.00467	−0.00114	Blattler & Diethelm (2007)
2454090.3271	−4895	0.00795	0.00214	Blattler & Diethelm (2007)
2454090.5155	−4894.5	0.00485	−0.00095	Blattler & Diethelm (2007)
2454097.2218	−4877	0.00862	0.00283	Blattler & Diethelm (2007)
2454097.4078	−4876.5	0.00312	−0.00266	Blattler & Diethelm (2007)
2454097.5998	−4876	0.00362	−0.00216	Blattler & Diethelm (2007)
2454114.2635	−4832.5	0.00675	0.00099	Blattler & Diethelm (2007)
2454114.4532	−4832	0.00495	−0.00081	Blattler & Diethelm (2007)
2454464.8998	−3917	0.00513	0.00003	Samec et al. (2011)
2454465.6656	−3915	0.00493	−0.00016	Samec et al. (2011)
2454465.8577	−3914.5	0.00553	0.00043	Samec et al. (2011)
2454466.8142	−3912	0.00452	−0.00056	Samec et al. (2011)
2454474.2857	−3892.5	0.00749	0.00242	Blattler & Diethelm (2007)
2455564.68610	−1045.5	0.00248	0.00059	Diethelm (2011)
2455947.68450	−45.5	−0.00067	−0.00103	Diethelm (2012)
2455886.78902	−204.5	0.00110	0.00047	The present paper
2455887.74401	−202	−0.00142	−0.00203	The present paper
2455964.15449	−2.5	0.00025	−0.00004	The present paper
2455965.11174	0	0.00000	−0.00029	The present paper
2455966.06924	2.5	0.00000	−0.00028	The present paper
2456603.18943	1666	−0.00289	−0.00018	The present paper
2456976.23106	2640	−0.00477	−0.00004	The present paper
2457394.08236	3731	−0.00816	−0.00094	The present paper
2458100.14163	5574.5	−0.01225	−0.00026	The present paper
2458109.14382	5598	−0.01060	0.00144	The present paper

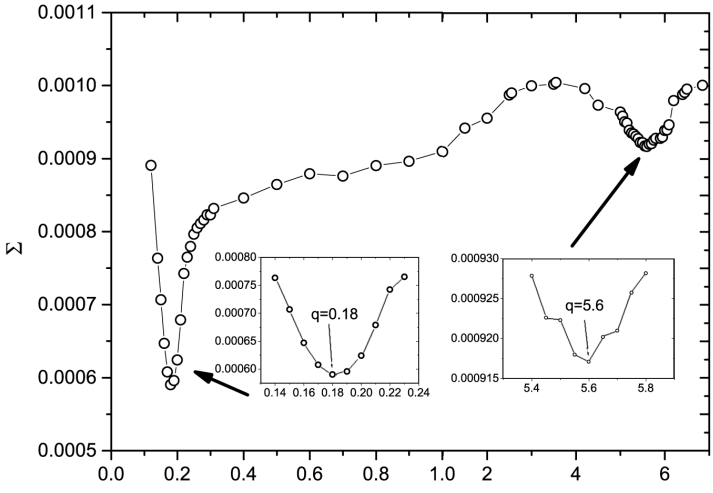

Fig. 4 The relation between Σ and q for V1853 Ori, and the minimum is found at $q = 0.18$.

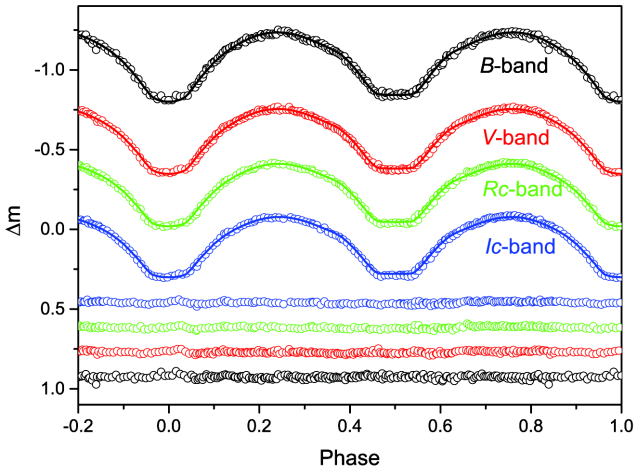

Fig. 5 Observed light curves of V1853 Ori in the B, V, Rc and Ic bands and their fits by theoretical light curves by using the W-D code.

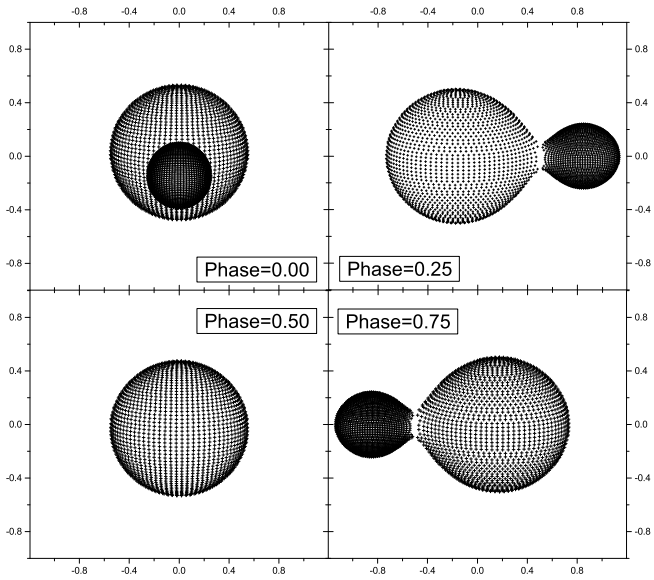

Fig. 6 Geometrical structure of the A-type intermediate contact binary V1853 Ori at phases 0.00, 0.25, 0.50 and 0.75.

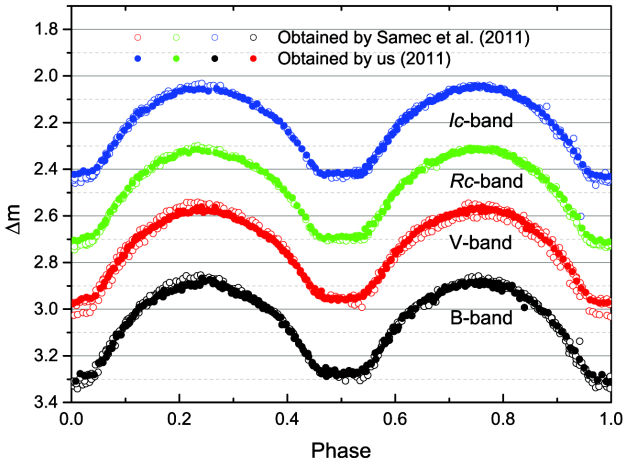

Fig. 7 A comparison of the two sets of B, V, Rc and Ic band light curves obtained by Samec et al. (2011) and by us. *Open circles* refer to data obtained by Samec et al. (2011), and *dots* indicate data obtained by us.

Table 9 Photometric Solutions Analyzed Using the W-D Code

Parameter	Photometric elements
Orbital inclination i	80.19(24)
Mass ratio m_2/m_1	0.1896(13)
Primary temperature T_1	6240 K
Temperature ratio T_2/T_1	0.9995(11)
Luminosity ratio $L_1/(L_1+L_2)$ in B band	0.81200(24)
Luminosity ratio $L_1/(L_1+L_2)$ in V band	0.81214(22)
Luminosity ratio $L_1/(L_1+L_2)$ in Rc band	0.81216(24)
Luminosity ratio $L_1/(L_1+L_2)$ in Ic band	0.81219(27)
Luminosity ratio $L_2/(L_1+L_2)$ in B band	0.18800(24)
Luminosity ratio $L_2/(L_1+L_2)$ in V band	0.18786(22)
Luminosity ratio $L_2/(L_1+L_2)$ in Rc band	0.18784(24)
Luminosity ratio $L_2/(L_1+L_2)$ in Ic band	0.18781(27)
Modified dimensionless surface potential of star 1	2.1663(44)
Modified dimensionless surface potential of star 2	2.1663(44)
Fillout factor	0.333(37)
Radius of star 1 (relative to semimajor axis) in pole direction	0.50066(83)
Radius of star 1 (relative to semimajor axis) in side direction	0.5490(12)
Radius of star 1 (relative to semimajor axis) in back direction	0.5742(13)
Radius of star 2 (relative to semimajor axis) in pole direction	0.2404(31)
Radius of star 2 (relative to semimajor axis) in side direction	0.2516(38)
Radius of star 2 (relative to semimajor axis) in back direction	0.2955(83)
Equal-volume radius of star 1 (relative to semimajor axis) R_1	0.54201(63)
Equal-volume radius of star 2 (relative to semimajor axis) R_2	0.2634(30)
Radius ratio R_2/R_1	0.4859(56)
$\Sigma\omega(O-C)^2$	0.000595

is decreasing at a rate of $dP/dt = -1.96(0.46) \times 10^{-7}\,\mathrm{d\,yr^{-1}}$. This is very common in contact binaries, such as V524 Mon ($dP/dt = -5.55 \times 10^{-8}\,\mathrm{d\,yr^{-1}}$, He et al. 2012), V532 Mon ($dP/dt = -1.716 \times 10^{-7}\,\mathrm{d\,yr^{-1}}$, He et al. 2016) and V1073 Cyg ($dP/dt = -2.24 \times 10^{-7}\,\mathrm{d\,yr^{-1}}$, Tian et al. 2018). The long-term decrease in the orbital period could be explained by mass transfer from the more-massive component to the less-massive one. As the orbital period is decreasing, V1853 Ori will evolve into a high fill-out overcontact binary. Finally, it will merge and produce a luminous red nova similar to that of V1309 Sco (e.g., Zhu et al. 2016).

Acknowledgements This work is partly supported by the National Natural Science Foundation of China (No. 11503077). CCD photometric observations of V1853 Ori were obtained with the 0.4-m telescope at Naresuan University in Thailand, and the 1-m and 60-cm R-C reflecting telescopes at Yunnan Observatories of the Chinese Academy of Sciences.

References

Binnendijk, L. 1964, AJ, 69, 154
Blattler, E., & Diethelm, R. 2007, Information Bulletin on Variable Stars, 5799
Chen, X., Deng, L., de Grijs, R., Wang, S., & Feng, Y. 2018, ApJ, 859, 140
Claret, A., & Gimenez, A. 1990, A&A, 230, 412
Cutri, R. M., Skrutskie, M. F., van Dyk, S., et al. 2003, VizieR Online Data Catalog, 2246
Diethelm, R. 2007, Information Bulletin on Variable Stars, 5781
Diethelm, R. 2009, Information Bulletin on Variable Stars, 5894
Diethelm, R. 2010, Information Bulletin on Variable Stars, 5920
Diethelm, R. 2011, Information Bulletin on Variable Stars, 5992
Diethelm, R. 2012, Information Bulletin on Variable Stars, 6029
Drilling, J. S., & Landolt, A. U. 2000, Normal Stars, Allen's Astrophysical Quantities, ed. A. N. Cox (New York: AIP Press; Springer), 381
Gaia Collaboration, Brown, A. G. A., Vallenari, A., et al. 2018, A&A, 616, A1
Gettel, S. J., Geske, M. T., & McKay, T. A. 2006, AJ, 131, 621
He, J.-J., & Qian, S.-B. 2008, ChJAA (Chin. J. Astron. Astrophys.), 8, 465
He, J.-J., Qian, S.-B., & Soonthornthum, B. 2016, AJ, 152, 120
He, J.-J., Wang, J.-J., & Qian, S.-B. 2012, PASJ, 64, 85
Høg, E., Fabricius, C., Makarov, V. V., et al. 2000, A&A, 355, L27
Hut, P. 1980, A&A, 92, 167
Lucy, L. B. 1967, ZAp, 65, 89
O'Connell, D. J. K. 1951, Publications of the Riverview College Observatory, 2, 85
Qian, S., & Yang, Y. 2005, MNRAS, 356, 765
Qian, S.-B., He, J.-J., Zhang, J., et al. 2017a, RAA (Research in

Astronomy and Astrophysics), 17, 087
Qian, S.-B., Han, Z.-T., Zhang, B., et al. 2017b, ApJ, 848, 131
Qian, S.-B., Zhang, J., He, J.-J., et al. 2018, ApJS, 235, 5
Ruciński, S. M. 1969, Acta Astronomica, 19, 245
Samec, R. G., Labadorf, C. M., Hawkins, N. C., Faulkner, D. R., & Van Hamme, W. 2011, AJ, 142, 117
Tian, X.-M., Zhu, L.-Y., Qian, S.-B., Li, L.-J., & Jiang, L.-Q. 2018, RAA (Research in Astronomy and Astrophysics), 18, 020
van Hamme, W. 1993, AJ, 106, 2096
Wilson, R. E., & Devinney, E. J. 1971, ApJ, 166, 605
Wilson, R. E. & Van Hamme, W. 2003, Computing Binary Stars Observables, the 4th Edition of the W-D Programe
Wilson, R. E., Van Hamme, W., & Terrell, D. 2010, ApJ, 723, 1469
Zhu, L.-Y., Zhao, E.-G., & Zhou, X. 2016, RAA (Research in Astronomy and Astrophysics), 16, 68